

14. Coleman, P. F.; Legg, J. I. *ibid.* 1970, 9, 937.
15. Drago, R. S. *Physical Methods in Chemistry*; Saunders, W. B. Philadelphia, 1977; pp 107-122
16. Basolo, F.; Ballhausen, C.; Bjerrum, J. *Acta Chem. Scand.* 1955, 810.
17. Shimura, Y.; Tsuchida, R. *Bull. Chem. Soc. Jpn.* 1956, 29, 311.
18. Halloran, L. J.; Legg, J. I. *Inorg. Chem.* 1974, 13, 2193.
19. Hidaka, J.; Igi, K.; Okabayashi, M. *Bull. Chem. Soc. Jpn.* 1979, 52, 753.
20. Denning, R. G.; Piper, T. S. *Inorg. Chem.* 1966, 5, 1056.

## Effect of Core Morphology on the Decomposition of $\text{CCl}_4$ over the Surface of Core/Shell Structured $\text{Fe}_2\text{O}_3/\text{MgO}$ Composite Metal Oxides

Hea Jin Kim, Jin Kang, Dong Gon Park\*, Ho-Jin Kweon†, and Kenneth J. Klabunde‡

*Department of Chemistry, Sookmyung Women's University, Seoul 140-742, Korea*

*†Samsung Display Devices Co. Ltd., Technology Div., Suwon 442-390, Korea*

*‡Department of Chemistry, Kansas State University, Manhattan, KS 66506 USA*

*Received May 1, 1997*

Core/shell structured composite metal oxides of  $\text{Fe}_2\text{O}_3/\text{MgO}$  were prepared by thermal decomposition of  $\text{Fe}(\text{acac})_3$  adsorbed on the surface of  $\text{MgO}$  cores. The morphology of the composites conformed to that of the  $\text{MgO}$  used as the cores. Broad powder X-ray diffraction peaks shifted toward larger  $d$ , large BET surface area ( $\sim 350 \text{ m}^2/\text{g}$ ), and the size of crystalline domains in nano range (4 nm), all corroborate to the nanocrystallinity of the  $\text{Fe}_2\text{O}_3/\text{MgO}$  composite which was prepared by using nanocrystalline  $\text{MgO}$  as the core. By use of microcrystalline  $\text{MgO}$  as the core, microcrystalline  $\text{Fe}_2\text{O}_3/\text{MgO}$  composite was prepared, and it had small BET surface area of less than  $35 \text{ m}^2/\text{g}$ . AFM measurements on nanocrystalline  $\text{Fe}_2\text{O}_3/\text{MgO}$  showed a collection of spherical aggregates ( $\sim 80 \text{ nm}$  dia) with a very rough surface. On the contrary, microcrystalline  $\text{Fe}_2\text{O}_3/\text{MgO}$  was a collection of plate-like flat crystallites with a smooth surface. The nitrogen adsorption-desorption behavior indicated that microcrystalline  $\text{Fe}_2\text{O}_3/\text{MgO}$  was nonporous, whereas nanocrystalline  $\text{Fe}_2\text{O}_3/\text{MgO}$  was mesoporous. Bimodal distribution of the pore size became unimodal as the layer of  $\text{Fe}_2\text{O}_3$  was applied to nanocrystalline  $\text{MgO}$ . The macropores in a wide distribution which the nanocrystalline  $\text{MgO}$  had were absent in the nanocrystalline  $\text{Fe}_2\text{O}_3/\text{MgO}$ . The decomposition of  $\text{CCl}_4$  was largely enhanced by the overlayer of  $\text{Fe}_2\text{O}_3$  on nanocrystalline  $\text{MgO}$  making the reaction between nanocrystalline  $\text{Fe}_2\text{O}_3/\text{MgO}$  and  $\text{CCl}_4$  be nearly stoichiometric. The reaction products were environmentally benign  $\text{MgCl}_2$  and  $\text{CO}_2$ . Such an enhancement was not attainable with the microcrystalline samples. Even for the nanocrystalline  $\text{MgO}$ , the enhancement was not attained, if not with the  $\text{Fe}_2\text{O}_3$  layer. Without the layer of  $\text{Fe}_2\text{O}_3$ , it was observed that the nanocrystalline domain of the  $\text{MgO}$  transformed into microcrystalline one as the decomposition of  $\text{CCl}_4$  proceeded on its surface. It appeared that the layer of  $\text{Fe}_2\text{O}_3$  on the particles of nanocrystalline  $\text{Fe}_2\text{O}_3/\text{MgO}$  blocked the transformation of the nanocrystalline domain into microcrystalline one. Therefore, in order to attain stoichiometric reaction between  $\text{CCl}_4$  and  $\text{Fe}_2\text{O}_3/\text{MgO}$  core/shell structured composite metal oxide, the morphology of the core  $\text{MgO}$  has to be nanocrystalline, and also the nanocrystalline domains has to be sustained until the core was exhausted into  $\text{MgCl}_2$ .

### Introduction

Nanophase materials have attracted scientist's interest, at first by stimulating a pure scientific curiosity, and lately because of unconventional applicability they may have. It has been well known that materials exhibit unexpected physical and chemical properties as the size of their particles get small down to a few nanometer range.<sup>1-7</sup> The properties observed for such nanophase materials have been shown to be quite different from the ones observed for their bulky counterparts, and this difference can be related to the fact that the fraction of the moieties exposed to the surface can no longer be negligible. Therefore, it has been proposed that

the surface chemistry on the nanophase materials should be prominently different from the one on the bulk, and ample experimental observations have shown that it is the case.<sup>8-10</sup>

For the study of the surface chemistry on metal oxides,  $\text{MgO}$  used to be a choice for the material, and both experimental and theoretical data on the material have been accumulated. Having a simple rock salt crystal structure, theoretical consideration is especially simple, and recent studies on modelling of oxide surface produced many results which are applicable to surface chemistry experimentally observed on  $\text{MgO}$ .<sup>11-14</sup> Perfect cubic shaped crystal of  $\text{MgO}$  has (100) crystalline facets exposed on its surface. Among the facets other than (100), the (111) facet is worth noticing. Experimental observations which were supported by ample theoretical considerations indicated that the (111) surface of

\*To whom correspondence should be addressed

MgO crystal is more reactive toward adsorbed chemicals than its (100) surface.<sup>12,13,15-19</sup> For example, it was shown that the chemisorption of small molecules, such as water or methanol, on (111) surface of MgO was preferred to that on (100) surface.<sup>[18]</sup> Hydrogen molecule was shown to dissociate on the (111) surface of MgO, whereas, it doesn't on (100) surface.<sup>17-19</sup> The higher reactivity of the (111) facet originates from low-coordinated ionic sites in such structures as steps, edges, kinks, valleys, and from defective sites such as vacancies, displaced ions.

The morphology of MgO particles is very dependent on how the actual specimen has been prepared.<sup>20,21</sup> This morphological difference was shown to be directly related to the chemistry on the surface of the material. It was observed that organophosphorus compounds dissociatively adsorbed on nanoscale particles of MgO, and phosphorus moieties were immobilized into the MgO.<sup>22,23</sup> Chlorocarbons were also shown to be destroyed on the surface of the nanocrystals of MgO, and the chlorines were immobilized into the MgO.<sup>24</sup> The high reactivity of the nanocrystalline MgO was related to the (111) surface exposed on spherical nanoparticles. When an overlayer of Fe<sub>2</sub>O<sub>3</sub> was applied on the nanocrystalline MgO, forming core/shell-type composite metal oxide, the reactivity toward chlorocarbons was observed to be largely enhanced.<sup>25,26</sup> It was observed that the nanocrystallinity of the sample was important in getting such enhancement. But, it appeared that the size in nano range was not a sole factor in enhancing the reactivity of the composite metal oxide toward chlorocarbons.

In this study, two MgO powder samples in extreme ends of possible morphologies which MgO can have were chosen. One kind was microcrystalline with its surface composed mostly of (100) facets, and the other was nanocrystalline with mostly (111) facets exposed. On each of those two different core MgO, an overlayer of Fe<sub>2</sub>O<sub>3</sub> was applied, and heat-treated into MgO/Fe<sub>2</sub>O<sub>3</sub> core/shell structured composite metal oxides. From ensuing comparison studies on those two composite samples, better understanding on the enhanced reactivity, which was brought by overlying the Fe<sub>2</sub>O<sub>3</sub> layer on the nanocrystalline MgO, has been sought.

## Experiments

**Syntheses.** Four different solid samples in two different morphological groups were prepared and were designated as CM-MgO, [Fe<sub>2</sub>O<sub>3</sub>]CM-MgO, AP-MgO, and [Fe<sub>2</sub>O<sub>3</sub>]AP-MgO. The prefix AP- and CM- came from 'aerogel prepared' and 'commercial'. First, two different MgO samples were prepared via different synthetic routes. One route was through Mg(OH)<sub>2</sub> aerogel gotten by supercritically drying<sup>27</sup> the Mg(OH)<sub>2</sub> alkogel, which produced nanocrystalline MgO (AP-MgO). The other route was via the hydration-dehydration of commercially available MgO, which produced microcrystalline MgO (CM-MgO). Using these two MgO samples in a very different morphology as the core, MgO/Fe<sub>2</sub>O<sub>3</sub> core/shell structured composite metal oxides were prepared by constructing an overlayer of Fe<sub>2</sub>O<sub>3</sub> over the core MgO. The layer of Fe<sub>2</sub>O<sub>3</sub> over the MgO was designated by putting [Fe<sub>2</sub>O<sub>3</sub>] in front of the prefix.

Mg turning (98%), calcined magnesia (MgO), and Fe

(acac)<sub>3</sub> (98%) were purchased from Aldrich, Fisher Scientific, and Strem, respectively. The methanol and toluene were dried over Mg(OMe)<sub>2</sub> and CaH<sub>2</sub> before use. THF and CCl<sub>4</sub> were both dried over activated (~150 °C, dynamic vacuum) molecular sieve.

Supercritical drying of aerogel was carried out in a 500 mL pressure reaction vessel (Parr Co.) which was equipped with a stirrer and a vent.

**CM-MgO.** After commercially purchased calcined magnesia was exposed to water saturated air for a day, the hydrated powder (2-3 g) was charged in a 100 mL Schlenk Reaction Vessel (SRV). Under dynamic vacuum (~10<sup>-3</sup> torr), the powder in the SRV was gradually heated up to 500 °C (it usually took 10 h) with 6 h hold at the temperature. Once the heat-treatment was finished, the sample was cooled to ambient temperature, and was kept under argon.

**AP-MgO.** In a three-way round bottom creased flask connected to argon, 100 mL of 1.0 M solution of Mg(OMe)<sub>2</sub> was prepared by reacting Mg turnings with dried methanol, and was well mixed with 300 mL dried toluene. While the solution was vigorously stirred, 4 mL distilled water was added over 30 min. As hydrolysis and condensation reaction proceeded, the solution became slightly turbid Mg(OH)<sub>2</sub> sol. The sol was further stirred for 10 h, and loaded in the 500 mL Parr-reactor. In the closed reactor, the sol was heated to 265 °C, and the pressure was maintained at 1000 psi. By opening the vent of the reactor, the solvent was expelled in its critical state, resulting in fluffy white powder of Mg(OH)<sub>2</sub> aerogel from the Mg(OH)<sub>2</sub> sol. About 2 g of the aerogel was loaded in the 100 mL SRV, and heated at 500 °C under dynamic vacuum as described in previous section.

**[Fe<sub>2</sub>O<sub>3</sub>]CM-MgO, [Fe<sub>2</sub>O<sub>3</sub>]AP-MgO.** An overlayer of Fe<sub>2</sub>O<sub>3</sub> was constructed on the MgO crystallites prepared in the previous sections. Over the solid samples of MgO (not exposed to the air, in SRV), whose surface was activated by heating in vacuum, a solution of Fe(acac)<sub>3</sub> in dried THF was added and stirred for 10 h. The MgO whose surface was covered by the adsorbed Fe(acac)<sub>3</sub> was filtered and dried. The dried powder was heated at 500 °C under dynamic vacuum, in the same manner as described earlier. After the heat treatment, the white color of the MgO turned pale gray ([Fe<sub>2</sub>O<sub>3</sub>]CM-MgO) to dark gray([Fe<sub>2</sub>O<sub>3</sub>]AP-MgO).

**Characterization.** Powder X-ray diffraction (PXRD) patterns were obtained with Scintag PAD-X diffractometer from the solid samples before and after the decomposition of CCl<sub>4</sub> was executed over them. FTIR spectra were taken by using Bio-Rad 3240 SPC, from pellets pressed from the mixture of KBr and the powder samples. Surface areas of the solid samples were measured by BET method, using Micrometrics Flowsorb II 2300. The N<sub>2</sub> adsorption-desorption isotherms were obtained with Quantachrom Adsorb-I-MP porosimeter. Physisorbed volatiles were removed from the powders by drying them at 300 °C under dynamic vacuum for 10 h before the measurements. Surface image was taken by AFM using Scanning Probe Microscope (SPM) Model M-30 (Wyco Co.) from a pellet made by pressing 0.1g of the powder at 11,000 psi. For monitoring the decomposition of CCl<sub>4</sub> on the surface of the powder samples, Gas Chromatograph model 530 from Gow-Mac was used with a SE-30 packed column and TCD. Temperature of oven and in-

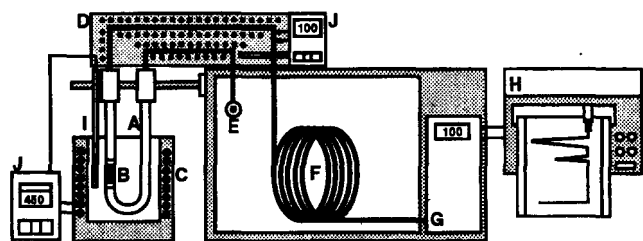


**Figure 1.** Schematic diagram showing GC device equipped with the *in situ* U-tube quartz reactor: (A) U-tube quartz reactor; (B) powder sample; (C) furnace; (D) heater; (E) injection port; (F) GC column; (G) detector; (H) recorder; (I) thermocouple; (J) temperature controller.

jector was 100 °C, and the flow rate of helium gas was 30  $\text{cm}^3/\text{min}$ . A U-tube quartz reactor (inner diameter of 7 mm) was attached between the injector and the entrance of the column, as shown in Figure 1. Powder sample, 100 mg, was loaded in the quartz reactor and immobilized by plugging both sides with ceramic wool. While the sample was heated at 425 °C by using small tube furnace, 1 L pulses of dried  $\text{CCl}_4$  were introduced over the solid sample in the reactor, with 7 min interval between pulses.

## Results

**Surface Area and Crystallite size.** Schematic diagram showing synthetic routes to four different powder samples is shown in Figure 2. Aerogel of  $\text{Mg}(\text{OH})_2$  was very fine fluffy powder which had high surface area of 700-800  $\text{m}^2/\text{g}$ . While it decomposed into AP-MgO at 500 °C in dynamic vacuum, the surface area diminished to 300-400  $\text{m}^2/\text{g}$  (which is still high value). Putting an overlayer of  $\text{Fe}_2\text{O}_3$  didn't change the surface area of the samples. XPS and Mössbauer analyses on the  $\text{Fe}_2\text{O}_3$  coated samples indicated the presence of highly dispersed  $\text{Fe}_2\text{O}_3$  layer on the core MgO.<sup>25,26</sup> Figure 3 shows PXRD patterns for  $[\text{Fe}_2\text{O}_3]\text{CM-MgO}$

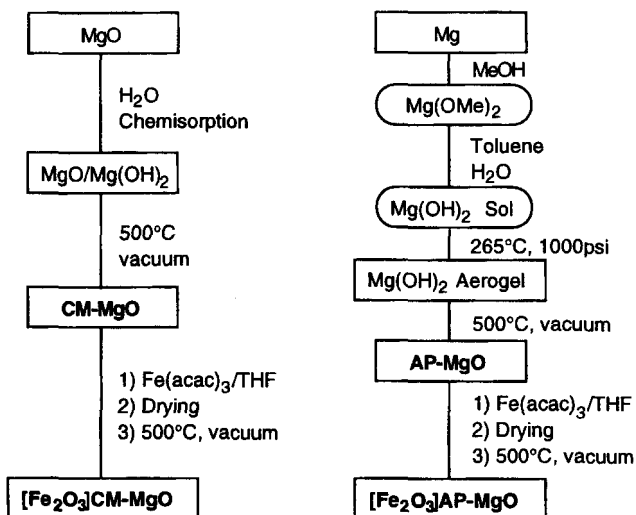


**Figure 2.** Schematic outline of the preparation of the solid samples. The AP-MgO and  $[\text{Fe}_2\text{O}_3]\text{AP-MgO}$  were prepared from the aerogel which was synthesized *via* a sol-gel route. The CM-MgO and  $[\text{Fe}_2\text{O}_3]\text{CM-MgO}$  were prepared from commercially purchased magnesia.

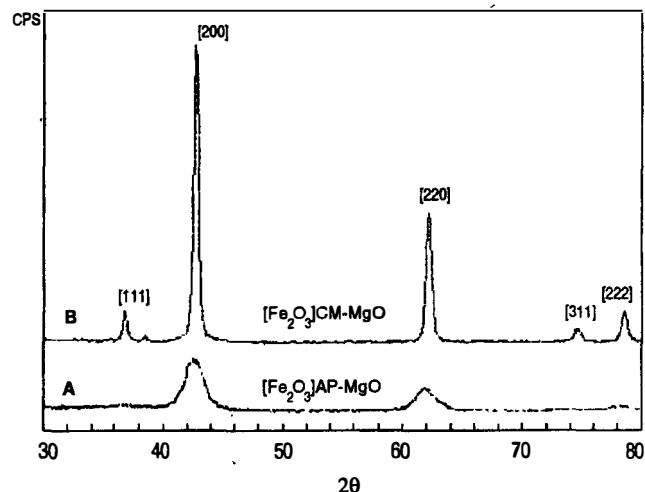


**Figure 3.** PXRD patterns of  $\text{Fe}_2\text{O}_3/\text{MgO}$  core/shell structured composites with different morphology: (A)  $[\text{Fe}_2\text{O}_3]\text{AP-MgO}$ ; (B)  $[\text{Fe}_2\text{O}_3]\text{CM-MgO}$ . Large half peak width of the diffractions from the  $[\text{Fe}_2\text{O}_3]\text{AP-MgO}$  indicates the nanocrystalline feature of it.

$\text{MgO}$  and  $[\text{Fe}_2\text{O}_3]\text{AP-MgO}$ . Nanocrystalline feature of the  $[\text{Fe}_2\text{O}_3]\text{AP-MgO}$  is apparent in the broadness of diffraction peaks. The size of the  $[\text{Fe}_2\text{O}_3]\text{AP-MgO}$  crystallites, which was calculated by the Scherer equation using the half peak width of the (200) diffraction at  $2\theta=42.5^\circ$ ,<sup>28</sup> was 40 Å, and the d value of its (200) diffraction was observed to be shifted ~0.15 Å larger than that of the  $[\text{Fe}_2\text{O}_3]\text{CM-MgO}$ , which is indicative of lattice strain presumably developed by nanocrystalline feature of the crystallites. The BET surface area of the  $[\text{Fe}_2\text{O}_3]\text{CM-MgO}$  was in a range of 10-35  $\text{m}^2/\text{g}$ , which was much smaller than that of the  $[\text{Fe}_2\text{O}_3]\text{AP-MgO}$  (350-370  $\text{m}^2/\text{g}$ ).

**Particle morphology.** Figure 4 and 5 show two dimensional surface feature of pellets pressed from powders of  $[\text{Fe}_2\text{O}_3]\text{CM-MgO}$  and  $[\text{Fe}_2\text{O}_3]\text{AP-MgO}$ . To compare relative roughness of the surface of the samples, force applied to the probe was maintained constant. On the AFM images, it was shown that the particles of the above two samples had very different morphology. The  $[\text{Fe}_2\text{O}_3]\text{CM-MgO}$  consisted of plate-like particles of ~50 nm thick, ~150 nm wide, and ~150 nm long (average size assessed from several three dimensional images). The apparent alignment of the crystallites was suggested to have occurred during the pellet-pressing. The possibility of the alignment be fake image was eliminated by getting the same alignment by cross-scanning on the same area. Contrary to the plate-like image of the  $[\text{Fe}_2\text{O}_3]\text{CM-MgO}$ , particles of the  $[\text{Fe}_2\text{O}_3]\text{AP-MgO}$  were shown to be spherical aggregates of ~80 nm diameter with very rough surface. The above observation of particles in different morphology is consistent to previous SEM/TEM observations performed on powder samples of CP-MgO, prepared by vacuum-heating hydrated CM-MgO (therefore, it should be close to CM-MgO), and of AP-MgO.<sup>9,29</sup> In the SEM/TEM observations, CP-MgO appeared as hexagonal platelets, and AP-MgO as irregular shaped aggregates.

Taking the AFM image of the  $[\text{Fe}_2\text{O}_3]\text{AP-MgO}$  gave fairly disturbing technical difficulty. Because of the roughness of the surface, the probe experienced sporadic jumps

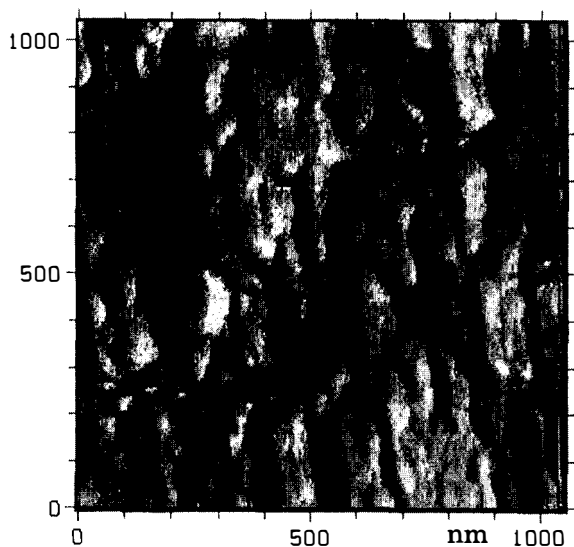


**Figure 4.** AFM micrograph of a pellet made by pressing  $[\text{Fe}_2\text{O}_3]$ CM-MgO powder.

which sometimes caused black-out of ensuing image. Unlike in the case of the  $[\text{Fe}_2\text{O}_3]$ AP-MgO, no such difficulty was experienced for the  $[\text{Fe}_2\text{O}_3]$ CM-MgO, and relatively smooth image was attained. This apparent difference of the surface roughness corroborates to BET surface area measurements, which showed the surface area of  $[\text{Fe}_2\text{O}_3]$ AP-MgO was about ten-fold larger than that of  $[\text{Fe}_2\text{O}_3]$ CM-MgO.

AFM images of CM-MgO and AP-MgO which did not have  $\text{Fe}_2\text{O}_3$  overcoat had same characteristic features of shape and roughness  $\text{Fe}_2\text{O}_3$  coated ones had. This observation suggests that basic topological features core MgO had were preserved even with overlayer of  $\text{Fe}_2\text{O}_3$ . It is well known that particle morphologies of MgO samples differ significantly depending on how the samples have been prepared.<sup>15,16</sup> When the growth of certain crystallographic plane

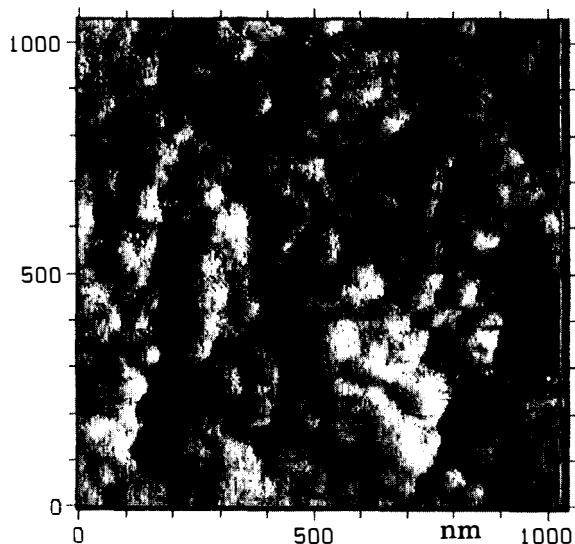


**Figure 5.** AFM micrograph of a pellet made by pressing  $[\text{Fe}_2\text{O}_3]$ AP-MgO powder.

was hindered or enhanced, resulting crystallites can be quite different in their shape.<sup>30</sup> For MgO, most of the flat surface of the hexagonal platelet-like crystallites of CM-MgO would be composed of (100) plane, whereas more proportion of the spherical surface of the AP-MgO would contain (111) plane.<sup>9,10,26</sup>

**Pore Characteristics.** The adsorption and desorption behavior of nitrogen on porous solids gives clues to the morphology and size distribution of the pores they have. In Figure 6, the  $\text{N}_2$  adsorption-desorption isotherms measured on the powder samples were provided. Isotherm curve for  $[\text{Fe}_2\text{O}_3]$ CM-MgO had a typical shape of type II which conformed to nonporous solid.<sup>31</sup> Apparently, no change in the feature was observed when the  $\text{Fe}_2\text{O}_3$  layer was applied over the CM-MgO (thereby, we show only one representative curve for  $[\text{Fe}_2\text{O}_3]$ CM-MgO in Figure 6-A). Isotherms

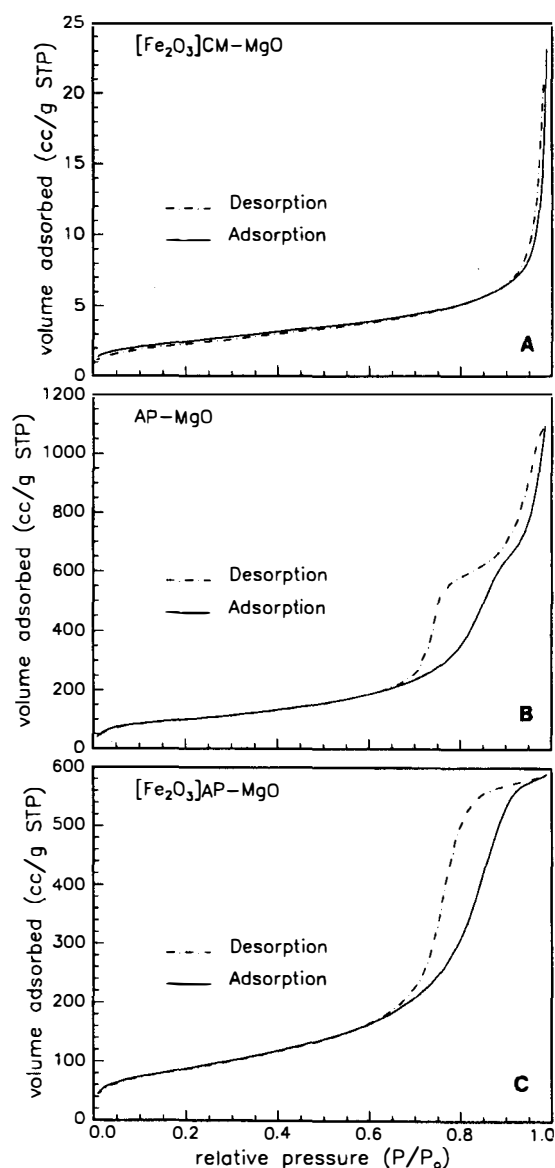
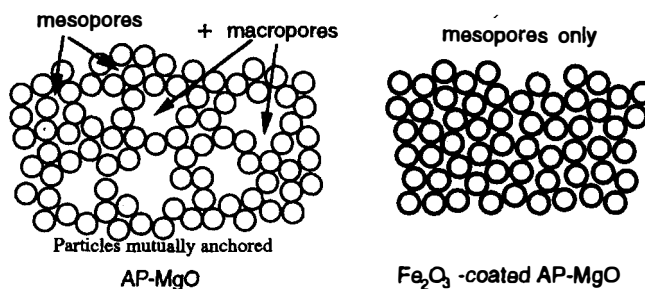


**Figure 6.** The nitrogen isotherms on powder samples of: (A)  $[\text{Fe}_2\text{O}_3]$ CM-MgO; (B) AP-MgO; (C)  $[\text{Fe}_2\text{O}_3]$ AP-MgO. The isotherm on CM-MgO was not shown because it was identical to the one on the  $[\text{Fe}_2\text{O}_3]$ CM-MgO.

for AP-MgO and  $[\text{Fe}_2\text{O}_3]\text{AP-MgO}$  exhibited the characteristic feature (type IV) of meso-porous solids.<sup>31</sup> Both samples had non-symmetric, inclined hysteresis loops, which indicated that the dimension of the pore was not monotonous, but rather 'necked'. The skewed loop in the isotherm of the AP-MgO, which appeared to be the overlap of two different segments, indicated the size distribution of the pore was bimodal. The shape of the hysteresis loop in lower pressure range is close to the type H2 which corresponds to the one for the 'necked' pores. The shape of the loop in higher pressure range fits better to the type H1 for the cylindrical pores.<sup>31</sup> Contrary to the CM-MgO, a significant change in the shape of the isotherm was observed as the  $\text{Fe}_2\text{O}_3$  layer was applied over the AP-MgO. Unlike in the isotherm of the AP-MgO, only one hysteresis loop was observed in the one for the  $[\text{Fe}_2\text{O}_3]\text{AP-MgO}$ , which indicated the bimodal distribution of the pores became unimodal as the  $\text{Fe}_2\text{O}_3$  layer was applied on the AP-MgO. Accumulative adsorbed volume curves were presented in Figure 7. The 'necking' is apparent in the mismatching feature of the adsorption and desorption curves. For both AP-MgO and  $[\text{Fe}_2\text{O}_3]\text{AP-MgO}$  the radius of the pore body, which was estimated from the adsorption curve, had a distribution width of around 100 Å, which was ranged from 70 to 170 Å. The radius of the 'neck', which was estimated from the desorption curve had a distribution width of around 20 Å, ranged from 70 to 90 Å. This estimation indicates that the pores in those two sam-



Scheme 1.

ples are typical cavities constructed when spherical particles are compacted in a bulk.<sup>31</sup> Also, it was shown that the feature in the macroporous region significantly changed as the  $\text{Fe}_2\text{O}_3$  layer was present. Whereas the AP-MgO had macropores in a fairly broad size range, roughly from 200 to 1000 Å, those macropores were nearly absent in the  $[\text{Fe}_2\text{O}_3]\text{AP-MgO}$ .

The edges, steps, kinks, and defects which are plenty on (111) facets of magnesium oxide surface were known to be readily converted to  $\text{Mg}(\text{OH})_2$  by chemisorbed water.<sup>32</sup> It was reported that the chemisorption of water took place even under very low pressure, and in an ambient condition it took less than 10 min.<sup>33</sup> Therefore, it is anticipated that the exposed surface of the spherical AP-MgO consists of hydroxides rather than oxides. It was speculated that the particles of the AP-MgO anchored to each other through the interaction among their hydroxylated surfaces, giving rise to the macropores in the AP-MgO, as shown in the Scheme 1. Because the layer of  $\text{Fe}_2\text{O}_3$  on the  $[\text{Fe}_2\text{O}_3]\text{AP-MgO}$  would not be easily hydroxylated, it was speculated that the particles of the  $[\text{Fe}_2\text{O}_3]\text{AP-MgO}$  were not effective in anchoring each other, and did not form the kind of the macropores the AP-MgO did.

**FTIR.** While solid samples of AP-MgO and, thereafter,  $[\text{Fe}_2\text{O}_3]\text{AP-MgO}$  were synthesized, FTIR spectra were taken, and presented in Figure 8. Relatively strong vibrational peaks which don't belong to metal-hydroxides were observed from the aerogel of  $\text{Mg}(\text{OH})_2$  at 1098, 2795, 2845, 2913  $\text{cm}^{-1}$  (Figure 8-A), which suggested the presence of residual methoxy groups.<sup>29</sup> This observation suggested that the hydrolysis during sol-gel reaction was incomplete, which left residual methoxy moieties in the aerogel. The residual carbon, ~2% by elemental analysis, in AP-MgO originated from these methoxy residues. After the aerogel was heat-treated at 500 °C, converting  $\text{Mg}(\text{OH})_2$  to  $\text{MgO}$ , the vibrational peaks of the methoxy moieties disappeared, and new peaks at 865, 1073, 1430, 1475, 1634  $\text{cm}^{-1}$  developed (Figure 8-B). These peaks correspond to unidentate carbonates and bicarbonates on the surface, suggested to be bound to lower coordinated magnesiums on edges and corners.<sup>10,34</sup> When  $\text{Fe}(\text{acac})_3$  was adsorbed on the activated surface of the AP-MgO, forming yellowish powders, peaks of acetylacetonates were observed at 921, 1020, 1194, 1264, 1409, 1462, 1520, 1610  $\text{cm}^{-1}$  (Figure 8-C). Compared to the peaks from the isolated  $\text{Fe}(\text{acac})_3$  [literature peak positions of isolated  $\text{Fe}(\text{acac})_3$ : 930(s), 1025(s), 1190(w), 1285(s), 1465(s), 1490(s), 1425(s), 1525(s), 1535(sh), 1555(sh), 1570(s), 1575(sh)  $\text{cm}^{-1}$ ],<sup>35</sup> the peaks from the Fe

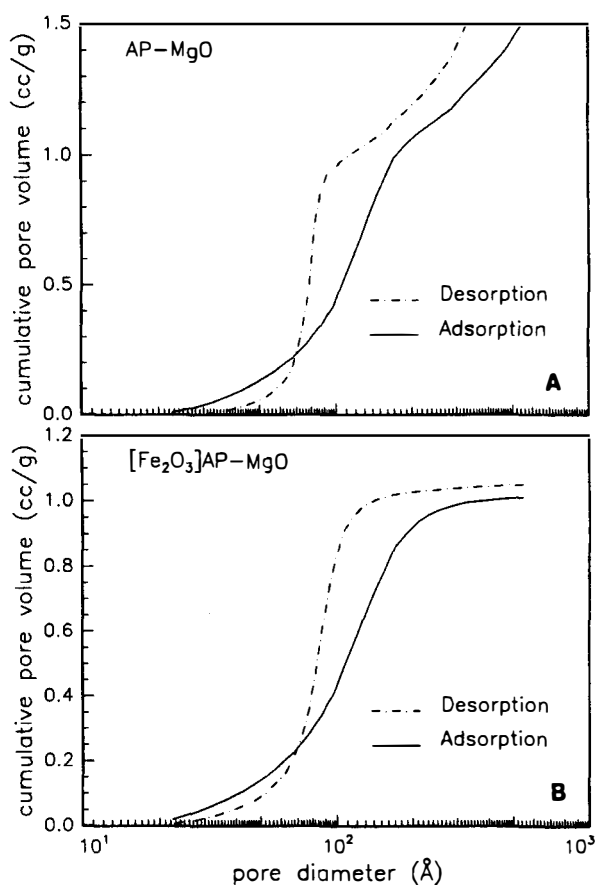


**Figure 7.** Cumulated pore volume of: (A) AP-MgO; (B)  $[\text{Fe}_2\text{O}_3]\text{AP-MgO}$ . The AP-MgO had macropores, whereas, they were absent in the  $[\text{Fe}_2\text{O}_3]\text{AP-MgO}$ .

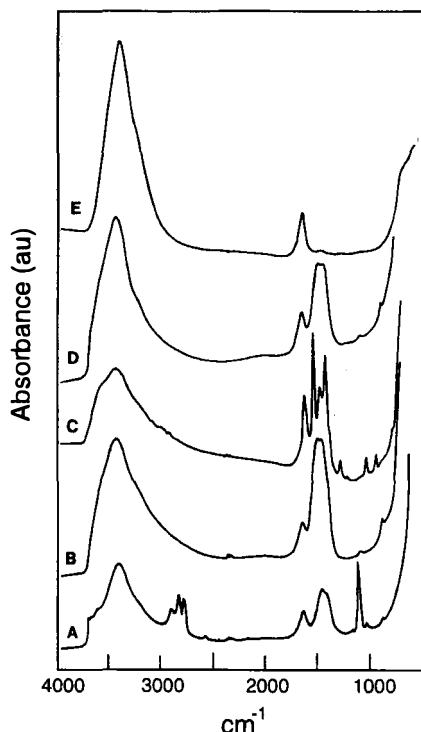


**Figure 8.** FTIR spectra of: (A)  $\text{Mg}(\text{OH})_2$  aerogel; (B) AP-MgO prepared by heat treating the  $\text{Mg}(\text{OH})_2$  aerogel; (C) AP-MgO whose the surface was covered by adsorbed  $\text{Fe}(\text{acac})_3$ ; (D)  $[\text{Fe}_2\text{O}_3]$ AP-MgO prepared by thermal decomposition of adsorbed  $\text{Fe}(\text{acac})_3$ ; (E) hygroscopic powder sample retrieved from the U-tube reactor after 0.1 g  $[\text{Fe}_2\text{O}_3]$ AP-MgO reacted with 100  $\mu\text{L}$

( $\text{acac}$ )<sub>3</sub> chemisorbed on the surface of the AP-MgO were observed to be shifted about 5–40  $\text{cm}^{-1}$  from those for the isolated one. As this yellowish powder turned to dark colored  $[\text{Fe}_2\text{O}_3]$ AP-MgO via decomposition of  $\text{acac}$  groups at 500 °C, the  $\text{acac}$  groups appeared to be converted to unidentate carbonates on the surface (from Figure 8-C to 8-D). Elemental analyses showed that the carbon content of the sample doubled to ~4.5%. The Fe content of the  $[\text{Fe}_2\text{O}_3]$ AP-MgO was 1.5%. On the contrary to the AP-MgO, the carbon content of CM-MgO was under the detection limit, and it increased to ~0.5% when  $\text{Fe}_2\text{O}_3$  layer was applied. The Fe content of  $[\text{Fe}_2\text{O}_3]$ CM-MgO was ~0.15%, which is ten-fold lower than the one for the  $[\text{Fe}_2\text{O}_3]$ AP-MgO. Considering the difference between BET surface area values (35 vs 350  $\text{m}^2/\text{g}$ ) of the samples, the amount of  $\text{Fe}(\text{acac})_3$  adsorptively loaded on the surface is closely related to the surface area of the MgO.

From the FTIR observation, it was suggested that the major components of the solids should be metal oxides, metal hydroxides, and metal carbonates. The empirical formulas based on the elemental analyses are  $\text{MgO}_{0.965}\text{C}_{0.018}\text{H}_{0.198}\text{Fe}_{7.17 \times 10^{-4}}$  and  $\text{MgO}_{1.66}\text{C}_{0.197}\text{H}_{1.175}\text{Fe}_{0.0141}$  for  $[\text{Fe}_2\text{O}_3]$ CM-MgO and  $[\text{Fe}_2\text{O}_3]$ AP-MgO, respectively. When these empirical formulas are rearranged into each components, presumed from the FTIR observations, they become  $\text{MgO}_{0.718}(\text{CO}_3\text{H})_{0.018}(\text{OH})_{0.180}(\text{Fe}_2\text{O}_3)_{7.17 \times 10^{-4}}$  and  $\text{MgO}_{0.048}(\text{CO}_3\text{H})_{0.197}(\text{OH})_{0.978}(\text{Fe}_2\text{O}_3)_{0.014}$  for the  $[\text{Fe}_2\text{O}_3]$ CM-MgO and the  $[\text{Fe}_2\text{O}_3]$ AP-MgO, respectively. It is quite possible that some of the carbon residues are elemental or existant as clusters.<sup>36</sup> Also,

some hydrogen must be originated from adsorbed water, especially for the AP-MgO which had high surface area. Substituting -OH into  $\text{H}_2\text{O}$  in the case, the empirical formula becomes  $\text{MgO}_{0.537}(\text{CO}_3\text{H})_{0.197}(\text{H}_2\text{O})_{0.489}(\text{Fe}_2\text{O}_3)_{0.014}$  for  $[\text{Fe}_2\text{O}_3]$ AP-MgO. Therefore, the above empirical formulas can not be the accurate ones. Still, it could be informative in the sense that a trend could be glimpsed on how the relative stoichiometry changes as the size of the crystallites decreases down to nano range. When the  $[\text{Fe}_2\text{O}_3]$ AP-MgO was compared to  $[\text{Fe}_2\text{O}_3]$ CM-MgO, it is shown that the amount of the lattice oxygen is about 15 fold smaller (0.048 compared to 0.718), whereas, the ones for the hydroxide and carbonate are 5.5 and 11 times larger (0.978 and 0.197 compared to 0.18 and 0.018, respectively). Therefore, as the surface area increased, and the size of the crystallites decreased, it was observed that the amount of the surfacial hydroxides and carbonates increased, compensated by the decrease of the lattice oxygens, which corroborates to the previous experimental results on the concentration of surfacial hydroxides.<sup>9</sup> This trend shows that as the size of the crystallites becomes smaller, and consequently as the surface area increases, the fractions of the surfacial components relative to the lattice oxygen dramatically increase, reflecting the diminished bulk property. As already noted in previous sections, the (200) PXRD peak of the  $[\text{Fe}_2\text{O}_3]$ AP-MgO was observed to be very broad, and the center of the diffraction was shifted toward larger  $d$  value, as much as 0.15 Å, which indicates the strain in the crystallites presumably caused by decreased bulk property.

**Decomposition of  $\text{CCl}_4$  on the surface.** Adsorptive dissociation of  $\text{CCl}_4$  on the surface of the samples was observed by monitoring effluent gas by GC after passing aliquots (pulses of 1  $\mu\text{L}$  each) of dried  $\text{CCl}_4$  over 100 mg of powdery samples heated in the quartz reactor at 425 °C in the flow of helium. The decomposition product was identified to be  $\text{CO}_2$  by MS. For effluent  $\text{CCl}_4$  (unreacted) and  $\text{CO}_2$ , the change of the GC peak area was graphically presented in Figure 9 and Figure 10. Putting the  $\text{Fe}_2\text{O}_3$  layer on the CM-MgO enhanced only a few initial decompositions (~2  $\mu\text{L}$ ); for the first pulse, the area ratio of  $\text{CO}_2/\text{CCl}_4$  was 1.92 and 5.37 for CM-MgO and  $[\text{Fe}_2\text{O}_3]$ CM-MgO, respectively. But, this enhancement became not that significant as more pulses of  $\text{CCl}_4$  were introduced, and the decomposition capacities of the above two samples appeared even to be reversed after the plateau was reached in the graph. At 10th pulse, for example, the area ratio of  $\text{CO}_2/\text{CCl}_4$  was 0.18 and 0.11 for the CM-MgO and the  $[\text{Fe}_2\text{O}_3]$ CM-MgO, respectively.

On the contrary to the case where the core was the CM-MgO, the decomposition of  $\text{CCl}_4$  was greatly enhanced by the  $\text{Fe}_2\text{O}_3$  layer over the AP-MgO: for  $[\text{Fe}_2\text{O}_3]$ AP-MgO, the breakthrough (the first detection of unreacted  $\text{CCl}_4$ ) occurred after 13–15 pulses. At 35  $\mu\text{L}$  injection, the area ratio of  $\text{CO}_2/\text{CCl}_4$  was 0.08 and 0.53 for the AP-MgO and the  $[\text{Fe}_2\text{O}_3]$ AP-MgO, respectively. Therefore, unlike in the case where the core was CM-MgO (see above), much more decomposition was observed over the  $[\text{Fe}_2\text{O}_3]$ AP-MgO even after the constant decomposition was reached.

Total of 100  $\mu\text{L}$   $\text{CCl}_4$  (100 pulses) was decomposed over each of the above samples until the decomposition reached constant level (plateau in the graph reached), and PXRD pat-

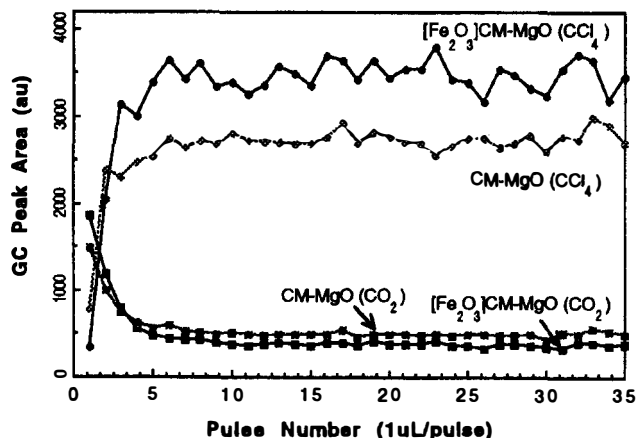


**Figure 9.** Integrated GC peak areas of the effluent volatiles. Pulses of CCl<sub>4</sub> (1  $\mu$ L/each) were passed over CM-MgO or [Fe<sub>2</sub>O<sub>3</sub>]CM-MgO heated at 425  $^{\circ}$ C.

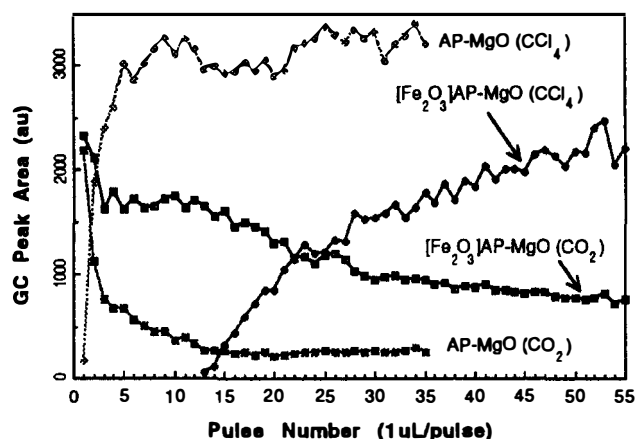


**Figure 10.** Integrated GC peak areas of the effluent volatiles. Pulses of CCl<sub>4</sub> (1  $\mu$ L/each) were passed over AP-MgO or [Fe<sub>2</sub>O<sub>3</sub>]AP-MgO heated at 425  $^{\circ}$ C.

terms were obtained from the powder samples which were retrieved from the quartz reactor, and shown in Figure 11. Corroborating to the GC observations described above, the conversion of MgO into MgCl<sub>2</sub> was almost complete for the [Fe<sub>2</sub>O<sub>3</sub>]AP-MgO, showing strong diffractions from hydrated MgCl<sub>2</sub>. On the contrary, most of the MgO diffractions were intact for the AP-MgO, indicating only a small fraction of the MgO was converted to MgCl<sub>2</sub>. In both cases, strong vibrational peak centered at 1637 cm<sup>-1</sup> was observed in the FTIR spectrum (Figure 8-E), which corresponds to the adsorbed water. The vibrational absorptions by carbonates, which were present before the decomposition reaction (Figure 8-B), were not observed. Presumably, as oxide surface turned into chloride, the carbonates bound to the surface were excluded, and water was adsorbed by hygroscopic MgCl<sub>2</sub> while the powdery sample was retrieved. Assuming 100% decomposition, about 120  $\mu$ L CCl<sub>4</sub> was calculated to be needed to convert 100 mg MgO completely into MgCl<sub>2</sub>. Therefore, by applying a thin layer of Fe<sub>2</sub>O<sub>3</sub> on the MgO, the decomposition of CCl<sub>4</sub> on the surface of [Fe<sub>2</sub>O<sub>3</sub>]AP-MgO could reach almost maximum efficiency, and the reaction between the [Fe<sub>2</sub>O<sub>3</sub>]AP-MgO and CCl<sub>4</sub>

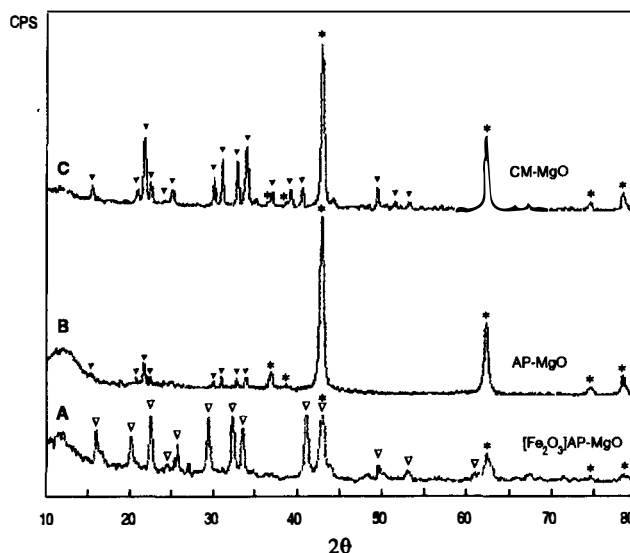


**Figure 11.** PXRD patterns of solid samples retrieved from the U-tube reactor after 100 pulses of CCl<sub>4</sub> were passed over: (A) [Fe<sub>2</sub>O<sub>3</sub>]AP-MgO; (B) AP-MgO; (C) CM-MgO. The marks are for ▼=MgCl<sub>2</sub>·6H<sub>2</sub>O, ▽=MgCl<sub>2</sub>·4H<sub>2</sub>O, and \*=MgO.

could be carried out almost as a stoichiometric reaction.

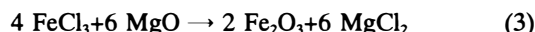
### Discussion and Speculation

What kind of driving force did the overlayer of Fe<sub>2</sub>O<sub>3</sub> on AP-MgO provided to enhance the destruction of CCl<sub>4</sub> on the surface of [Fe<sub>2</sub>O<sub>3</sub>]AP-MgO in such a large extent? The exhaustive understanding on the exact mechanism has not been attained, yet. Though, some plausible explanations can be speculated on the basis of the experimental observations gotten so far.

When CCl<sub>4</sub> decomposed *via* reaction (1) on the surface of AP-MgO, the surface layer converted into MgCl<sub>2</sub>.



The amount of liquid CCl<sub>4</sub> needed to cover the surface of 100 mg solids which have surface area of 300 m<sup>2</sup>/g as a monolayer is calculated to be a few  $\mu$ L. Therefore, first two or three pulses of CCl<sub>4</sub> would be all is needed to turn most of the surfacial MgO into MgCl<sub>2</sub>. Regeneration of an oxide surface should rely only to a diffusion process. But, if the Fe<sub>2</sub>O<sub>3</sub> overlayer was present over the MgO, a fresh oxide surface could be regenerated *via* facile Cl<sup>-</sup>/O<sub>2</sub><sup>-</sup> ion exchange, which was represented by reaction (2) and (3), occurring through the Fe<sub>2</sub>O<sub>3</sub>-MgO solid-solid interface.



The driving force for the ion exchange reaction would originate from the fact that iron oxide ( $\Delta G = -742$  KJ/mol) is thermodynamically more stable than chloride counterpart ( $\Delta G = -334 \times 2 = -668$  KJ/mol), whereas magnesium oxide ( $\Delta G = -570$  KJ/mol) is less stable than its chloride counterpart ( $\Delta G = -592$  KJ/mol). By considering the iron remained after the reaction to CCl<sub>4</sub>, it was suggested that the

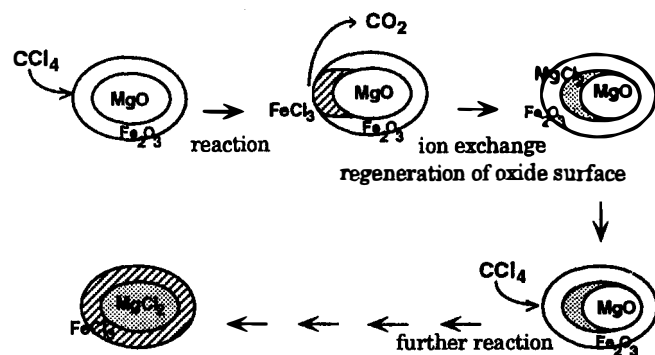
reaction (2) did not proceed to completion. Reaction intermediate could be  $\text{FeOCl}$  which was reported to be produced when a mixture of  $\text{Fe}_2\text{O}_3$  and  $\text{FeCl}_3$  was heated to 350 °C. Thermodynamic data on the compound are not available.

The mechanism for the decomposition of  $\text{CCl}_4$  on the surface of the  $[\text{Fe}_2\text{O}_3]\text{AP-MgO}$ , deducible from the above argument was suggested in Scheme 2. It can be anticipated that the diffusion process in the  $\text{MgO}$  core moiety should eventually influence the ion exchange through the solid-solid interface. As expected, it was observed that the breakthrough was delayed by increasing the interval between pulses.<sup>25</sup>

In part, the enhanced  $\text{Cl}^-/\text{O}_2^-$  ion exchange reaction described above may explain the observed stoichiometric reaction between  $[\text{Fe}_2\text{O}_3]\text{AP-MgO}$  and  $\text{CCl}_4$ . But, it fails in the case of  $\text{CM-MgO}$  and  $[\text{Fe}_2\text{O}_3]\text{CM-MgO}$ , where the  $\text{Fe}_2\text{O}_3$  layer over the  $\text{CM-MgO}$  apparently diminished the overall amount of  $\text{CCl}_4$  converted to  $\text{CO}_2$ . Therefore, some additional factors should also be counted on to understand the enhanced reactivity observed in  $[\text{Fe}_2\text{O}_3]\text{AP-MgO}$ .

The amount of Fe loaded on the surface of the samples increased proportionally to the increase of the surface area, which indicated the thickness of the  $\text{Fe}_2\text{O}_3$  layer should not be much different over  $\text{CM-MgO}$  or  $\text{AP-MgO}$ . The experimental observations described in previous sections, such as size of the crystallites in nano range, rough-surfaced aggregates observed by AFM, compositional decrease of bulk oxides deduced from FTIR and elemental analyses, lattice strain observed on PXRD pattern, all point to the nanocrystalline characteristics of  $\text{AP-MgO}$  and  $[\text{Fe}_2\text{O}_3]\text{AP-MgO}$ , which were comparable to the microcrystalline features of  $\text{CM-MgO}$  and  $[\text{Fe}_2\text{O}_3]\text{CM-MgO}$ . Therefore, it is certain that the unusual reactivity of the  $[\text{Fe}_2\text{O}_3]\text{AP-MgO}$  toward  $\text{CCl}_4$  originates partly from the nanocrystallinity of the core  $\text{MgO}$ .

One other factor which should be considered is the kind of the crystalline facets exposed on the surface. As already noted in the other articles,<sup>9,10,26</sup> the strikingly different shape of the particles indicated that the major facets of the plate-shaped  $\text{CM-MgO}$  should mostly be (100) plane, whereas round-shaped  $\text{AP-MgO}$  should have more (111) plane on its surface. There are ample experimental observations and theoretical calculations which showed that the  $\text{MgO}$  (100) plane is relatively inert toward chemical reactions on its surface, whereas the  $\text{MgO}$  (111) plane is fairly reactive toward chemicals adsorbed on its surface.<sup>12,13,17-21</sup> The theoretical calculations showed that low-coordinated surface sites in steps, edges, and valleys which are plenty on (111) plane



would act as the reactive sites in the reaction on the surface. Therefore, the  $\text{AP-MgO}$  and the  $[\text{Fe}_2\text{O}_3]\text{AP-MgO}$  in spherical particle shape, which should have higher concentration of reactive sites than in the plate-like  $\text{CM-MgO}$ , would exhibit higher reactivity toward adsorbed chemicals.

If this factor which was described above were a major one, it should be applicable not only to the  $[\text{Fe}_2\text{O}_3]\text{AP-MgO}$ , but also to the uncoated  $\text{AP-MgO}$ . In Figure 12, the adsorptive decompositions of  $\text{CCl}_4$  observed by GC over  $\text{CM-MgO}$  and  $\text{AP-MgO}$  (uncoated) were compared. Initially (till second pulses), it was observed indeed that more  $\text{CCl}_4$  decomposed on the  $\text{AP-MgO}$  than on the  $\text{CM-MgO}$ , as expected on the basis of the kind of major crystalline facets exposed on their surface. But, the decomposition capacity was observed to reverse after third pulses (marked by asterisk), and once the plateau on the graph was reached, it was observed that actually the  $\text{AP-MgO}$  destroyed less amount of  $\text{CCl}_4$  than the  $\text{CM-MgO}$ . This observation is opposite to the expectation based on the particle morphology. In the Figure 11 which shows PXRD patterns taken from powder samples retrieved from the quartz reactor after 100  $\mu\text{L}$  of  $\text{CCl}_4$  was decomposed over them at 425 °C, the relative intensity of the diffractions from the hydrated  $\text{MgCl}_2$  (compared to  $\text{MgO}(200)$  diffraction) appeared much smaller in the  $\text{AP-MgO}$  than in the  $\text{CM-MgO}$ , which corroborates to the above GC observations. How could this discrepancy be rationalized?

A peculiar feature which should be noticed in the above PXRD pattern of the  $\text{AP-MgO}$  retrieved after the GC experiment (Figure 11-B) was the fact that the diffractions from remaining  $\text{MgO}$  were observed to be much sharper than before the GC experiment. The PXRD peaks of the  $\text{AP-MgO}$  taken before the GC experiment was almost identical to the one for the  $[\text{Fe}_2\text{O}_3]\text{AP-MgO}$  (for comparison, see the Figure 3-A) and they were very broad. Apparently, the broad diffraction peak of the nanocrystalline  $\text{AP-MgO}$  somehow became narrower after 100  $\mu\text{L}$   $\text{CCl}_4$  was decomposed over the same sample, which suggests that the nanocrystalline  $\text{MgO}$  transformed into microcrystalline one. On the contrary to the uncoated  $\text{AP-MgO}$ , it could be seen that the  $\text{MgO}$  diffractions (see [222] and [220] diffractions at

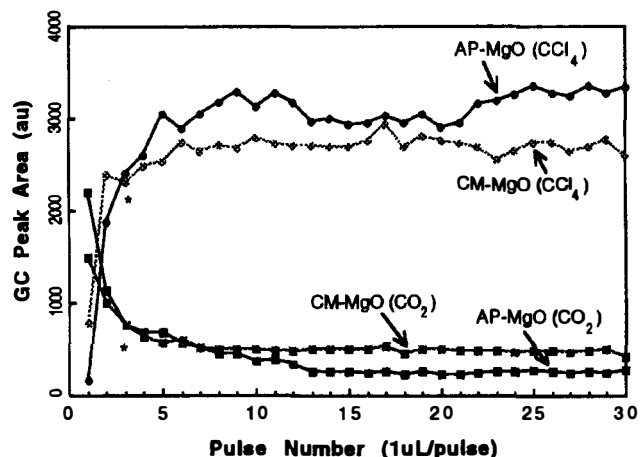
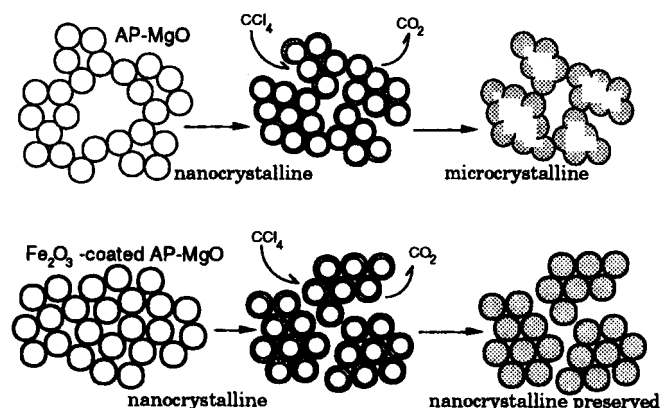


**Figure 12.** Integrated GC peak areas of the effluent volatiles. Pulses of  $\text{CCl}_4$  (1  $\mu\text{L}$ /each) were passed over  $\text{AP-MgO}$  or  $\text{CM-MgO}$  heated at 425 °C.



$2\theta=78$  and  $62^\circ$ ) in the Figure 11-A, which was for the remaining core MgO after 100  $\mu\text{L}$  of  $\text{CCl}_4$  was decomposed over the  $[\text{Fe}_2\text{O}_3]\text{AP-MgO}$ , appeared still as broad peaks. This observation indicates that the nanocrystalline feature of the  $[\text{Fe}_2\text{O}_3]\text{AP-MgO}$  persisted even after the GC experiment. The BET surface area of the samples was observed to decrease in large extent, if once  $\text{CCl}_4$  was decomposed over their surface.<sup>26</sup> These observations suggest that the  $\text{Fe}_2\text{O}_3$  layer over the nanocrystalline AP-MgO blocked the transformation of nanocrystalline core MgO into microcrystalline one, when the macroscopic restructuring (the collapse of the pore structure accompanied by drop of the surface area) was triggered by the decomposition of  $\text{CCl}_4$  over the samples. In the Scheme 3, difference in the outcomes of the restructuring, which was presumed to be caused by the presence of the  $\text{Fe}_2\text{O}_3$  layer over the nanocrystalline AP-MgO were schematically suggested.

As noted in earlier section on the pore characteristics, the contact among the particles of the AP-MgO appeared to be more intimate than among those of the  $[\text{Fe}_2\text{O}_3]\text{AP-MgO}$ . By considering melting point of  $\text{MgCl}_2$  ( $714^\circ\text{C}$ ) is much lower than that of  $\text{MgO}$  ( $2826^\circ\text{C}$ ),  $\text{MgCl}_2$  phase will be much more mobile than  $\text{MgO}$  phase. Therefore, upon the formation of exterior layer of  $\text{MgCl}_2$ , the particles of the AP-MgO would coalesce into a few larger aggregates. In order for the aggregate to become a single microcrystal, reorientation of lattice atoms should occur. If the initial crystalline domains were microcrystalline, energetically, this kind of reorientation wouldn't be plausible. But, considering the crystallites of the AP-MgO were nanocrystalline, the atomic reorientation could well occur during the inter-diffusion of  $\text{Cl}^-$  and  $\text{O}_2^-$  ions (the lattice strain observed by PXRD should play a role). On the contrary, when the  $\text{Fe}_2\text{O}_3$  layer was present on the particles of the AP-MgO, the nanocrystallites would have less chance to coalesce. In the  $\text{N}_2$  adsorption-desorption experiment described in the earlier section, the particles of the AP-MgO was shown to form macropores. In order to form the macropores, the particles of AP-MgO should be mutually anchored, as shown in the above scheme, presumably through interaction among hydroxylated moieties on their surface. On the contrary, absence of macropores in the  $[\text{Fe}_2\text{O}_3]\text{AP-MgO}$  suggested that contact among the particles of the  $[\text{Fe}_2\text{O}_3]\text{AP-MgO}$  became less significant by the presence of the  $\text{Fe}_2\text{O}_3$  overlayer.



Scheme 3.

Even though the particles of the  $[\text{Fe}_2\text{O}_3]\text{AP-MgO}$  should coalesce each other, the layer of  $\text{Fe}_2\text{O}_3$  would anyway act as a barrier to hinder the transformation of many nanocrystalline domains into a single microcrystalline one *via* atomic reorientation. Therefore, for the particles of the  $[\text{Fe}_2\text{O}_3]\text{AP-MgO}$ , the nanocrystalline domains should be preserved even though the overall structure collapsed, which would corroborate to the PXRD and porosimetry observations. Therefore, it was suggested that the nanocrystalline characteristics of the AP-MgO were preserved by the  $\text{Fe}_2\text{O}_3$  overlayer while the decomposition of  $\text{CCl}_4$  (followed by the inter-diffusion of lattice anions) proceeded. This preservation of the nanocrystallinity of the AP-MgO by  $\text{Fe}_2\text{O}_3$  overlayer is suggested to be one of major factors which made the reaction between  $[\text{Fe}_2\text{O}_3]\text{AP-MgO}$  and  $\text{CCl}_4$  be almost stoichiometric.

### Conclusion

By putting an overlayer of  $\text{Fe}_2\text{O}_3$  on nanocrystalline MgO (AP-MgO), forming core/shell type composite oxides ( $[\text{Fe}_2\text{O}_3]\text{AP-MgO}$ ), almost stoichiometric reaction between MgO and  $\text{CCl}_4$  could be carried out at  $425^\circ\text{C}$ , producing environmentally benign  $\text{MgCl}_2$  and  $\text{CO}_2$ . Using the microcrystalline MgO as the core, the stoichiometric reaction could not be carried out even though the  $\text{Fe}_2\text{O}_3$  layer was applied. The nanocrystalline morphology of the core MgO appeared to be one of essential factors in attaining the enhanced reactivity toward  $\text{CCl}_4$ . Necessary condition for the  $\text{Fe}_2\text{O}_3/\text{MgO}$  core/shell type composite oxide to have such a high reactivity toward  $\text{CCl}_4$  was not appeared to be met only by having nanocrystalline core. Experimental observations suggested that the nanocrystallinity of the core MgO should be preserved while  $\text{CCl}_4$  decomposed over the surface to keep such a high reactivity toward  $\text{CCl}_4$ . The overlayer of  $\text{Fe}_2\text{O}_3$  on the nanocrystalline core MgO apparently disturbed the coalescence among MgO nanocrystallites, preserving the nanocrystalline domains of the core until most of the core MgO transformed into  $\text{MgCl}_2$ . Thereby, the unusually high reactivity of the  $\text{Fe}_2\text{O}_3$  coated nanocrystalline MgO toward  $\text{CCl}_4$  was maintained until the core MgO was almost totally exhausted. When the overlayer of  $\text{Fe}_2\text{O}_3$  was not applied, the MgO particles apparently coalesced into bigger one, and atomic reorientation occurred, turning nanocrystalline domains into microcrystalline ones, during macroscopic structural change caused by the decomposition of  $\text{CCl}_4$ . With this transformation of the crystallinity, the reactivity of the MgO toward  $\text{CCl}_4$  diminished in large extent.

It was demonstrated that the reactivity of metal oxide toward chlorocarbons could be maximized on nanocrystalline core/shell-structured  $\text{Fe}_2\text{O}_3/\text{MgO}$  composite metal oxide. This type of composite materials could be a good candidate for safe disposal of environmentally problematic chlorocarbons. Because the waste of chlorocarbons used to be incinerated at high temperature, they generate intractable byproducts of  $\text{HCl}$  and  $\text{Cl}_2$ . In this regard, immobilizing chlorides into benign solid products would provide a possible way to subdue the generation of the volatile chlorinated byproducts.

**Acknowledgment.** The support of the Korean Science and Engineering Foundation (961-0306-065-2) is acknow-

ledged with gratitude. In part, this work was supported by the Basic Science Research Institute Program-Ministry of Education (BSRI-96-3404), and by Hazardous Substance Research Center at Kansas State University.

### References

1. Easom, K. A.; Klabunde, K. J.; Sorenson, C. M.; Hadjipanayis, G. C. *Polyhedron* **1994**, *13*, 1197.
2. Klabunde, K. J.; Zhang, D.; Glavee, G. N.; Sorenson, C. M.; Hadjipanayis, G. C. *Chem. Mater.* **1994**, *6*, 784.
3. Goldstein, A. N.; Echer, C. M.; Alivisatos, A. P. *Science* **1992**, *256*, 1425.
4. Johansson, K. R.; McLendon, G.; Marchetti, A. P. *Chem. Phys. Lett.* **1991**, *179*, 321.
5. Wang, Y.; Herron, N. *Phys. Rev. B* **1990**, *42*, 7253
6. Andres, R. P.; Averback, R. S.; Brown, W. L.; Brus, L. E.; Goddard, W. A., III; Kaldor, A.; Louie, S. G.; Moskovits, M.; Peercy, P. S.; Riley, S. J.; Siegel, R. W.; Spaepen, F.; Wang, Y. *J. Mater. Res.* **1989**, *4*, 704.
7. Honeycutt, J. D.; Andersen, H. C. *J. Phys. Chem.* **1987**, *91*, 4950.
8. Koper, O.; Li, Y. X.; Klabunde, K. J. *Chem. Mater.* **1993**, *5*, 500.
9. Itoh, H.; Utampanya, S.; Stark, J. V.; Klabunde, K. J.; Schulp, J. V. *Chem. Mater.* **1993**, *5*, 71.
10. Stark, J. V.; Park, D. G.; Lagadic, I.; Klabunde, K. J. *Chem. Mater.* **1996**, *8*, 1904.
11. Kantorovich, L. N.; Holender, J. M.; Gillan, M. J. *Surf. Sci.* **1995**, *343*, 221.
12. Refson, K.; Wogelius, R. A.; Fraser, D. G.; Payne, M. C.; Lee, M. H.; Milman, V. *Phys. Rev. B* **1995**, *52*, 10823.
13. Langel, W.; Parrinello, M. *J. Chem. Phys.* **1995**, *103*, 3240.
14. Scamehorn, C. A.; Hess, A. C.; McCarthy, M. I. *J. Chem. Phys.* **1993**, *99*, 2786.
15. Scamehorn, C. A.; Harrison, N. M.; McCarthy, M. I. *J. Chem. Phys.* **1994**, *101*, 1547.
16. Onishi, H.; Egawa, C.; Aruga, T.; Iwasawa, Y. *Surf. Sci.* **1987**, *191*, 479.
17. Bauschlicher, C. W., Jr.; Lengsfeld, B. H., III; Liu, B. *J. Chem. Phys.* **1982**, *77*, 4084.
18. Karim, M.; Vidali, G. *Phys. Rev. B* **1989**, *39*, 3854.
19. Sawabe, K.; Koga, N.; Morokuma, K.; Iwasawa, Y. *J. Chem. Phys.* **1994**, *101*, 4819.
20. Morris, R. M.; Klabunde, K. J. *Inorg. Chem.* **1983**, *22*, 682.
21. Knözinger, E.; Jacob, K. H.; Singh, S.; Hofmann, P. *Surf. Sci.* **1993**, *290*, 388.
22. Li, Y. X.; Schlup, J. R.; Klabunde, K. J. *Langmuir* **1991**, *7*, 1394.
23. Li, Y. X.; Koper, O.; Atteya, M.; Klabunde, K. J. *Chem. Mater.* **1992**, *4*, 323.
24. Koper, O.; Li, Y. X.; Klabunde, K. J. *Chem. Mater.* **1993**, *5*, 500.
25. Klabunde, K. J.; Khaleel, A.; Park, D. *High Temp. Mater. Sci.* **1995**, *33*, 99.
26. Klabunde, K. J.; Stark, J.; Koper, O.; Mohs, C.; Park, D. G.; Decker, S.; Jiang, Y.; Lagadic, I.; Zhang, D. *J. Phys. Chem.* **1996**, *100*, 12142.
27. Teichner, S. J.; Nicolaon, G. A.; Vicarini, M. A.; Gardes, G. E. *Advances in Colloid and Interface Science* **1976**, *5*, 245.
28. West, A. R. *Solid Chemistry and Its Application*; John Wiley & Sons: New York, U. S. A., 1984; p 174.
29. Utampanya, S.; Klabunde, K. J.; Schlup, J. R. *Chem. Mater.* **1991**, *3*, 175.
30. West, A. R. *Solid Chemistry and Its Application*; John Wiley & Sons: New York, U. S. A., 1984; p 11.
31. Gregg, S. J.; Sing, K. S. W. *Adsorption, Surface Area and Porosity*; Academic press: London, U. K., 1982; p 111.
32. Jones, C. F.; Reeve, R. A.; Rigg, R.; Segall, R. L.; Smart, R. S. C.; Turner, P. S. *J. Chem. Soc., Faraday Trans.* **1984**, *80*, 2609.
33. Duński, H.; Joźwiak, W. K.; Sugier, H. *J. Catal.* **1994**, *146*, 166.
34. Evans, J. V.; Whateley, T. L. *Trans. Faraday Soc.* **1967**, *63*, 2769.
35. Sadtler, High Resolution Spectra of Inorganics and Related Compounds, Sadtler Research Laboratories, Inc., Y333.
36. A broad ESR resonance centered at 3440 gauss was observed, which suggests the carbon clusters (unpublished results by authors).